RF Compressor (SLED) Phase-Modulation to Reduce Peak Fields in the MAX IV Linear Accelerator

JOEL EKSTRÖM
MASTER´S THESIS
DEPARTMENT OF ELECTRICAL AND INFORMATION TECHNOLOGY
FACULTY OF ENGINEERING | LTH | LUND UNIVERSITY

RF Compressor (SLED) Phase-Modulation to Reduce Peak Fields in the MAX IV Linear Accelerator

Joel Ekström
jo5472ek-s@student.lu.se

Department of Electrical and Information Technology
Lund University

Supervisors: Daniel Sjöberg & Robert Lindvall

Examiner: Mats Gustafsson

June 2, 2023

© 2023
Printed in Sweden
Tryckeriet i E-huset, Lund

Abstract

Modern particle accelerators need strong electric fields in order to produce high energy particles. Such high voltages are typically reached by injecting pulsed radio frequency power through several steps of amplification. At the end, pulse compression is used to further improve the energy gain at the cost of pulse-length. A typical pulse compression method developed at the Stanford Linear Accelerator Center (SLAC) is the SLAC Energy Doubler (SLED), which modulates the outgoing wave-envelope using either the phase or amplitude of the incoming wave.

Normal operation of the cavity dictates that the phase is shifted 180° at the final part of the pulse. This thesis, however, aimed to explore alternative operation modes in order to reduce the peak field of the output while retaining as much of the energy gain as possible. Previous work was examined and a suitable, linear phase-modulation was chosen to be implemented.

In order to realize the modulation scheme, an appropriate phase-shifter and logic controller were chosen and tested in order to determine how the new system would affect phase-stability. Results seemed to indicate that the new system would have no major impact on this parameter. It was then deemed appropriate to install the system on one of the accelerating sections towards the end of the MAX IV linear accelerator.

Results from the newly installed setup seemed to conform with the modelling work despite certain setbacks caused by the cavities inside the SLED being out of tune. Overall the implementation appears to have accomplished its task well.

Acknowledgements

Before continuing I would like to acknowledge the people who have made this thesis possible and in no small part contributed to its finalization. Firstly I would like to thank everyone from the RF-group at MAX IV for helping me throughout the practical parts of this project. In particular I would like to thank:

- Robin Svärd for lending a hand with installation and management of the new phase-shifter system as well as offering helpful advice when I needed it.
- Robert Lindvall for supervising the project from MAX IV and offering possible ways forward throughout the implementation process.
- Dionis Kumbaro for mentoring me and offering the summer work which eventually led to the idea of doing this thesis. Also for allowing me to use his office.

A special thanks also goes out to my uncle Anders Larsson, for getting me interested in engineering and helping me get in contact with Dionis.

I would like to extend gratitude towards Daniel Sjöberg, for agreeing to supervise this project from LTH and offering much needed advice when it came to writing and structuring the thesis.

My friends also deserve recognition for their support and for making my time at LTH much more fun than stressful. I wish I could name you all and everything you have done for me but this thesis would have doubled in size by the time I was done listing half of it.

Finally I would like to thank my family. I could not have done it without your support!

Popular Science Summary

The modern world is dependent on our understanding of nature and how both organisms and materials behave on the very smallest of scales. Whether the goal is to create better concrete, batteries or vaccines one needs to understand how things move and form in order to make way for improvements. This is why many turn to particle accelerators, not for the particles they accelerate but from what those particles produce.

At MAX IV electrons are used to produce very bright and fine X-rays which are capable of resolving details down to the atomic level in some cases. These electrons need to be accelerated up to almost the speed of light. In order to achieve this they are sent down a tube throughout which they are fed energy by an injected electric field at certain stages. This field is, in fact, a radio frequency wave which has been amplified up to several kilovolts in order to boost the electrons as much as possible.

In order to achieve this level of amplification however, the field is stored in a cavity referred to as a SLED. This cavity can be likened to a water tank where the timing or phase of the incoming radio-wave is the equivalent to the valve. When the phase is instantly shifted 180° the stored field empties quickly and you get a short but intense burst which decays quickly. This is similar to immediately opening the valve completely.

The problem with this method however, is that the peak field strength becomes so high that there is a risk of discharge in the transmission line which can damage the equipment. This can be mended by instead shifting the phase over some short period of time which smooths over the initial spike in the burst. Correct modulation still delivers almost the same energy amount to the electron beam.

This master's thesis has explored the concept of phase-modulation and how such a system could be implemented at the MAX IV accelerator. Several mathematical models of the process were set up and after discussion with the MAX IV staff, a suitable phase-modulation scheme was chosen. Appropriate electronic components were then decided upon and tested in order to determine if their precision and capabilities were good enough. Finally the system was implemented and the results appeared similar to what was predicted by the mathematical models.

Table of Contents

List of Figures

List of Tables

Chapter 1
Introduction

The need for probing the very small is today something which extends beyond the realm of high energy physics and into many different scientific fields. In order to realize experiments on these scales, one often turns to particle accelerators capable of producing the electromagnetic waves needed. It is then of the highest importance to guarantee safe, effective and stable operation of the associated accelerator facilities, and be able to further develop the field of accelerator physics in order to meet future demands. The standard approach to particle acceleration is today that of injecting radio frequency (RF) waves into the accelerating structure via cavities. So-called klystron amplifiers are used in order to increase the field strength and transfer as much energy as possible [1].

A common technique used to improve the energy gain is that of pulse compression via external cavities situated in the transmission line between amplifier and accelerating structure. Developed at the Stanford Linear Accelerator Center (SLAC), these cavities are known as SLAC energy doublers (SLED), and are designed to retain the beginning part of the signal. When the latter part of the incoming wave is phase-reversed the compressed pulse is then released [2]. The outgoing signal is thus able to deliver higher power over a shorter time. However, as the peak field increases the risk of damaging equipment and even breakdown of the transmission line becomes more likely. In order to mitigate wear, phase-modulation of the wave has been proposed in order to smooth over the outgoing compressed wave, which would lower the energy gain somewhat but also reduce the peak fields. This project aims to realize such a phase-modulation technique while also taking into consideration how the phase-stability of the system would be affected.

1.1 Background and Motivation

Located on the outskirts of Lund, MAX IV is what is known as a synchrotron radiation facility. It utilizes electrons accelerated to high energies (1.5 GeV/3 GeV) in order to produce coherent X-rays of very high flux and low spread, often referred to as brilliance [3, Ch. 12.2.]. These facilities enable research in a variety of fields including medicine, biology, chemistry and material science, making them invaluable tools in the pursuit of developing our knowledge and understanding.

The high energy electron beam is achieved by injecting $\sim 4\,\mu$s long pulsed RF-

power into the accelerating structure as electrons pass through, thereby ”feeding” the beam [4]. This is primarily achieved at the linear accelerator (LINAC) through the use of RF-amplifying klystrons in a manner similar to what was mentioned earlier. The LINAC itself can be seen in Figure 1.1 along with a general overview of the MAX IV facility. The SLED-cavity construction allows for the build-up of RF-power over a certain period of time, before being released by phase-shifting the incoming wave 180° almost instantaneously. The result is a compressed wave about 1 µs in length with a much higher peak field comparatively [2].

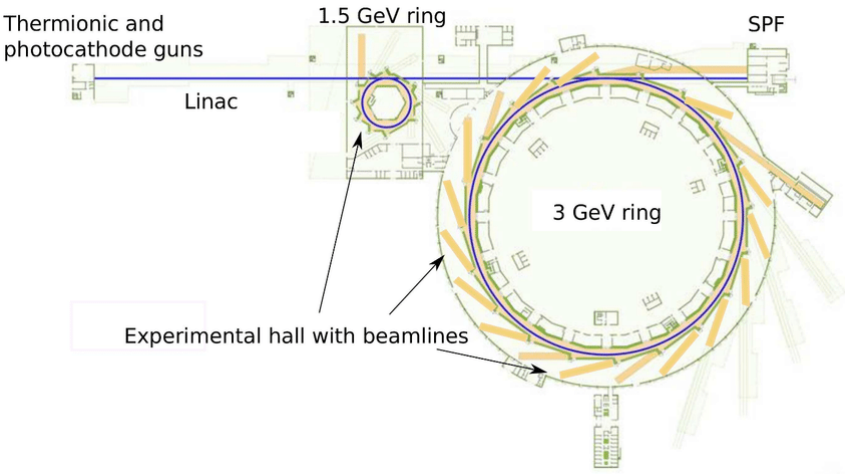

Figure 1.1: Overview of the MAX IV facility. Drawing by Johnny Kvistholm.

There are however issues arising from increasing the peak field such as the risk of arcing which in turn can cause breakdown of the transmission. By changing the phase-modulation to a linear transition over time, it has been shown that reducing the peak field while retaining most of the energy gain is possible.

1.2 Project Aims and Main Challenges

The aim with this thesis project was to reduce peak fields in the power transmission while also minimizing losses in the energy transferred to the electrons. This would be done by improving the low-level RF control to make smooth phase-transitions. The goal would be to model and develop a phase-modulator in order to allow for a stable phase-shift in the RF-power being fed into the SLED-cavity. An evaluation of the new system with regards to phase-stability would also be desirable in order to compare with the previous iteration.

The main challenges included finding an appropriate phase-transition model as well as redesigning the current phase-shift system. Phase-stability measurements would also need to be made in order to evaluate the practicality of the implementation. Some difficulties were expected in regards to access for testing

and evaluation due to the current energy crisis of 2022/2023 potentially forcing temporary shutdowns of the MAX IV facility.

1.3 Related Work

Investigations into reducing the peak field have already been made which led to the idea of modulating the phase during the 180° transition. A solution to be used for the FERMI free electron laser (FEL) was proposed by Wang et. al. where the modulation scheme was changed to an initial jump to a phase-degree ϕ_0. This was followed by a linear transition until a 180° change was achieved [5]. The results were later implemented and tested by Serpico et. al. yielding at best a 20% reduction in the peak field, while only a loss of about 1% in the energy gain [6]. It was acknowledged, however, that a flatter compressed pulse could be obtained utilizing a non-linear phase-modulation scheme instead.

Alternative investigations have also been made into amplitude-modulation of the incoming wave after the 180° phase-shift [7]. Simulations yielded similar results as for phase-modulation, however issues were mentioned when considering implementation. This was due to the non-linear behaviour of the klystron at the operating saturation regime (see Section 2.1.4). For this reason amplitude-modulation will not be considered for implementation in this project as the klystrons are already operating close to this regime. It bears mentioning however, that these solutions are also being developed and implemented. Christou et. al. describe the initial implementation of such a scheme for the Diamond Light Source pre-injector LINAC [8]. The injected pulse was tuned by hand in order to circumvent non-linearities and initial results seem promising, however, further implementation is pending at the time of writing.

1.4 Methodology

The thesis project was based at the MAX IV accelerator where the current phase-modulation system was evaluated along with a literature study in order to deepen understanding of the subject. A new model was then developed using simulation tools in order to determine an appropriate phase-shift scheme. Desired results of the model was based on consultation with the MAX IV RF-group.

The system was then translated into component-form using previous work from the literature study as a base. Consideration was given to what components could be reused and how the new system was best implemented to fit MAX IV. Finally the model was implemented and measurements of phase-stability were made on a test-bench before installing it into the transmission line. Appropriate wave-forms of the SLED and related components could then be recorded and analyzed.

1.4.1 Limitations

Some limitations to the scope of the thesis were considered. Firstly, implementation and testing were limited to one accelerating unit due to the limited down-time

of the MAX IV facility. Further motivation would come from the potential shutdowns due to the energy crisis at the time of the thesis work being conducted. This is not believed to have had a major effect on the results as the hardware is close to identical for all units.

The accelerating unit in question was located at the end of the LINAC and was chosen so as to not disturb operation of the rest of the facility. Unfortunately due to the recentness of its installation, the vacuum of the unit had to be conditioned during testing and could thus not be run at ideal conditions. Furthermore it was discovered that the SLED-cavity itself had deviated from resonance and had to be adjusted mechanically. For lack of time testing proceeded anyway but results were potentially affected.

Due to time-constraints as well as the aforementioned uncertainty of implementation, effects on the beam dynamics were neither considered for discussion nor for testing. This was also done to keep the focus of the project on RF and SLED rather than accelerator design. Potential changes to beam quality were thus not evaluated.

Chapter 2
Theory

In order to understand the problem at hand the necessary theory must first be presented concerning how energy is provided to the beam in the MAX IV injector LINAC. The details of both transmission line and phase-modulation are discussed along with options for implementation. In Section 2.1, a general overview is given for how the beam is started and fed via RF Units, detailing the role of the klystron and cavities. Section 2.2 discusses how pulse compression is achieved and how SLED can be viewed through this perspective. In Section 2.3, the SLED-cavity is discussed in detail including its structure as well as the fundamental equations necessary. Finally, in Section 2.4, different phase-modulation schemes are presented along with real world implementation options.

2.1 Transmission

While not necessary to the mathematical modelling performed in later chapters, this section discussing the transmission line will establish essential concepts related to modern particle acceleration.

2.1.1 General Overview

The simplest way to accelerate a beam of charged particles would be to apply a direct electric field between two points in space and allow the beam to propagate between [3]. When trying to achieve a higher beam energy however, this implementation becomes impractical as the field strength needs to increase. This in turn leads to a heightened risk of arcing. Instead most high energy accelerators today, including MAX IV, inject an alternating field into a portion of the accelerating structure. The challenge then is to ensure that the beam of particles arrives in phase with the field.

As previously mentioned MAX IV uses a LINAC to produce high energy electrons for the storage rings where synchrotron radiation is extracted. Electrons are provided by either a thermionic gun or a photocathode where they are extracted in bunches. They are then accelerated through 19 accelerating sections consisting of two 5.2 m long S-band (2.9985 GHz) LINAC structures and one RF unit [4, Ch. 4.1]. The RF units themselves provide power to the accelerating structures but are also found supplying power to both injector guns. They consist of a solid state

modulator powering a klystron amplifier (see Section 2.1.4) which in turn connects to the SLED-cavity (see Section 2.3) via waveguides. The layout of an accelerating section can be seen in Figure 2.1.

The modulator supplies a roughly 6 µs long pulse (HV Out) which powers the klystron, allowing for the amplification of the 4 µs RF-pulse (RF in/out) that also passes through the device. Due to its immense field strength (around 300 kV), the signal requires waveguides with vacuum as medium ($< 10^{-8}$ bar) in order to transport the strong electric field into the SLED-cavity [4, Ch. 4.6]. The cavity compresses the pulse, however, due to the structure of the system some initial power passes through immediately. A roughly 1 µs long compressed pulse is then emitted at the end, carrying up to 2.5 times the field strength at its peak. This system is capable of supplying the electron beam with 95 MeV per pulse.

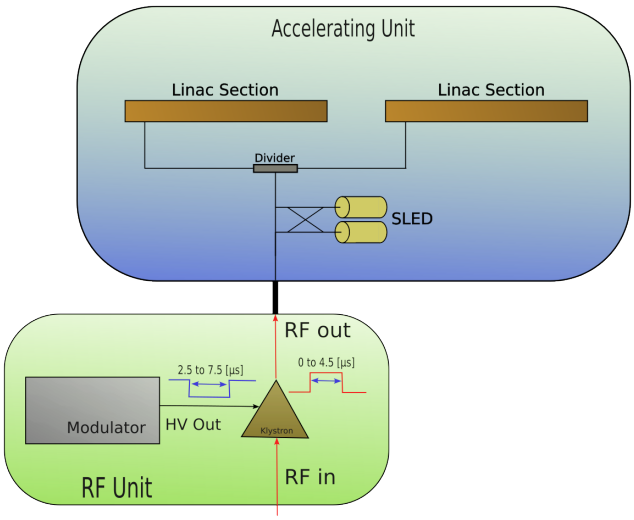

Figure 2.1: Layout of an accelerating section of the linear accelerator at MAX IV [4, Ch. 4.6]. RF is fed and modulated at the RF in port, amplified by the klystron and sent forward (RF out) into the SLED and accelerating unit.

2.1.2 Waveguides

In order to connect the different parts of the transmission line, rectangular metal waveguides are used which allow the RF-pulse to propagate in a single direction [9, Ch. 9.5]. Assuming no imperfections in the transmission and no fields present within the waveguide material, we are able to set up boundary conditions

$$\begin{cases} \boldsymbol{E}^{\parallel} = 0 \\ \boldsymbol{B}^{\perp} = 0 \end{cases} \tag{2.1}$$

within the structure. $\boldsymbol{E}^{\parallel}$ denotes the tangential components of the electric field $\boldsymbol{E}$, and $\boldsymbol{B}^{\perp}$ denotes the normal component of the magnetic flux density $\boldsymbol{B}$. We also note that since the waves propagate in a single direction (along the z-axis)

$$\begin{cases} \boldsymbol{E}(x,y,z,t) = \boldsymbol{E}_0(x,y)e^{i(kz-\omega t)} \\ \boldsymbol{B}(x,y,z,t) = \boldsymbol{B}_0(x,y)e^{i(kz-\omega t)} \end{cases} \tag{2.2}$$

By now solving Maxwell's equations we are able to obtain conditions for the longitudinal components

$$\begin{cases} [\frac{\partial^2}{\partial x^2} + \frac{\partial^2}{\partial y^2} + (\frac{\omega}{c})^2 - k^2]E_z = 0 \\ [\frac{\partial^2}{\partial x^2} + \frac{\partial^2}{\partial y^2} + (\frac{\omega}{c})^2 - k^2]B_z = 0 \end{cases} \tag{2.3}$$

where c is the speed of light and k the wave number in the z-direction. The waveguides and SLED-cavities of the MAX IV transmission line are designed for so-called transverse electric (TE) waves, meaning $E_z = 0$. Solving for B_z in this case, with a waveguide of dimensions a and b yields

$$B_z = B_0 \cos\frac{m\pi x}{a} \cos\frac{n\pi y}{b} \tag{2.4}$$

Here m and n are arbitrary integers meaning this type of wave has modes TE_{mn}, see Figure 2.2 for an example. The wave number k can also be determined to be

$$k = \sqrt{\left(\frac{\omega}{c}\right)^2 - \pi^2\left[\left(\frac{m}{a}\right)^2 + \left(\frac{n}{b}\right)^2\right]} \tag{2.5}$$

from which we note that there exist modes TE_{mn} for which k becomes imaginary. Such cases would result in the wave seen in (2.2) becoming exponentially decaying meaning there is a cut-off frequency for which waves do not propagate. The cut-off frequency can be determined as

$$f_c = \frac{c}{2}\sqrt{\left(\frac{m}{a}\right)^2 + \left(\frac{n}{b}\right)^2} \tag{2.6}$$

from which we also note that at least one of the indices must be non-zero.

2.1.3 Accelerating Cavities

The final step of the transmission line is the LINAC where the energy from the injected RF is transferred to the electron beam. The process takes place in the accelerating cavities and depending on the accelerator, they are either found throughout the whole structure or only at certain parts. In the case of the MAX IV LINAC the cavities make up most of the S-band structures, see Figure 2.3.

The principles of such an accelerating structure build on the idea of either a travelling wave or a stationary wave filling up the cavities, in order to accelerate

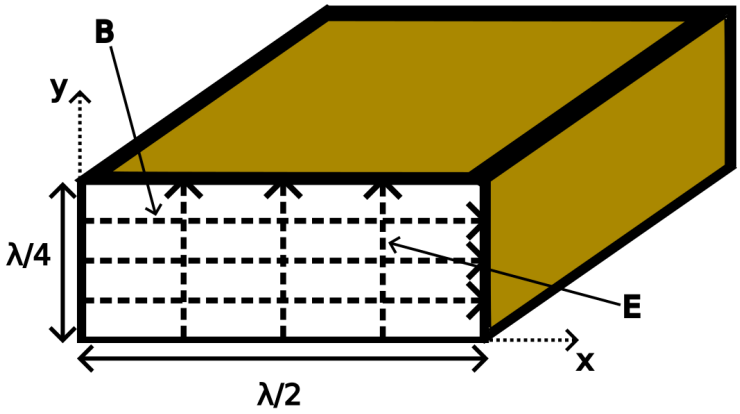

Figure 2.2: Illustration of mode TE_{10} inside a rectangular waveguide with the transverse fields depicted as arrows with dashed lines.

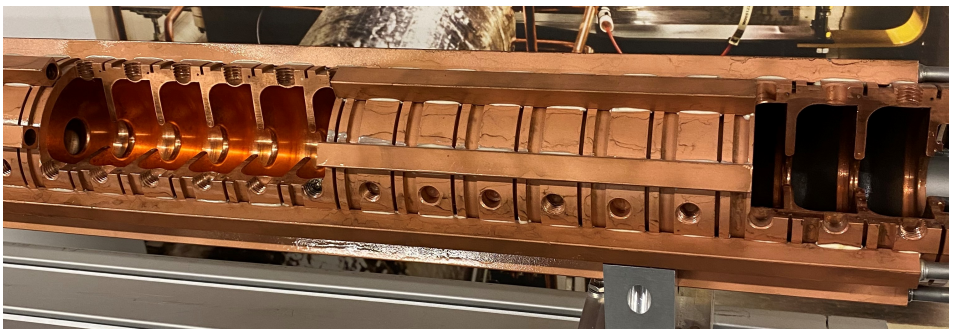

Figure 2.3: Cross-section of an S-band accelerating structure.

the particles traveling through the center [3, Ch. 4]. The MAX IV LINAC uses the former where the injected RF-wave is made to propagate along the structure, using the cavity-sizes as obstacles to influence the group-velocity [4, Ch. 4.6]. Due to the electron bunch quickly becoming relativistic, the bunch-velocity is fairly constant throughout most of the structure meaning the phase will also remain constant. This is what enables most of the LINAC-structures to be constructed in the exact same way. Note also that the energy left in the RF-wave after one accelerating structure is absorbed at the end by absorbent material. This can be seen in Figure 2.3 as the black coating at the right end.

In a similar manner to the waveguides, cavities can be described using Maxwell's equations [10]. In the case of a closed off cylindrical cavity in vacuum, the boundary conditions at the capped off ends can be determined as, in cylindrical coordinates,

$$\begin{cases} \dfrac{\partial E_z(\boldsymbol{\rho}, 0)}{\partial z} = \dfrac{\partial E_z(\boldsymbol{\rho}, d)}{\partial z} = 0 \\ B_z(\boldsymbol{\rho}, 0) = B_z(\boldsymbol{\rho}, d) = 0 \end{cases} \tag{2.7}$$

using the transverse coordinate $\boldsymbol{\rho} = (x, y)$. We now observe that fields inside the cavity will have contributions from waves propagating in both positive and negative z-directions. Thus the wave number k will depend on the 3-dimensional geometry of the cavity, meaning we have to introduce 3 arbitrary integers n, m and l. The TE modes of the cavities are thus most often referred to as TE_{mnl} which can be shown to have resonance frequencies

$$f_c = \frac{c}{2\pi}\sqrt{\left(\frac{\eta_{mn}}{a}\right)^2 + \left(\frac{l\pi}{d}\right)^2} \tag{2.8}$$

where d is the length of the cavity and a the radius [10]. η_{mn} is the n^{th} zero to $J'_m(\rho)$ which is the derivative of the m^{th} Bessel function[1] with function variable $\rho = |\boldsymbol{\rho}|$.

As mentioned previously, the accelerating cavities do not, in fact, have closed off ends but instead tiny holes through which the RF-wave can propagate. It also bears mentioning that since particles need to be accelerated in the longitudinal plane, the TE modes become impractical since $E_z = 0$. Instead transverse magnetic (TM) waves are used where the condition $B_z = 0$ is valid.

Let us assume these hollow caps are an equal distance L from one another and describe the propagating electric field using Floquet's theorem [11]. The theorem states that at a given frequency, the wave-function is multiplied by a constant between periods. We also assume that no single mode can satisfy the boundary conditions but must instead be described using a series of harmonics

$$\begin{cases} E_z(r, z, t) = F(r, z)e^{i(k_0 z - \omega t)} \\ F(r, z) = F(r, z + L) \\ F(r, z) = \sum_n a_n(r)e^{i(2\pi n/L)z} \end{cases} \tag{2.9}$$

[1] Further reading can be found in Microwave theory by Karlsson and Kristensson [10, Ch. 5, 6].

where a_n are some unknown radial functions, and k_0 refers to the Floquet wave number of the injected RF [11].

For a traveling wave accelerating cavity as used in MAX IV, the situation is dominated by the mode $n = 0$ [11], and the corresponding harmonic of the electric field is noted as E_{z0}. In order to keep $E_{z0} \approx$ const, a constant gradient of cavity dimensions along the propagation direction is applied. The Floquet wave number is typically determined from an eigenvalue problem taking the exact geometry of the unit cell into account, and defines two velocities: the phase velocity $v_{\mathrm{ph}} = \omega/k_0$ and the group velocity $v_{\mathrm{g}} = d\omega/dk_0$. The condition for acceleration is to find a phase velocity which matches that of the electrons (close to the speed of light), whereas the group velocity can be further analyzed using the power relation

$$v_g(z) = -\frac{\omega P(z)}{Q dP/dz} \tag{2.10}$$

in which, $P(z)$ refers to the power throughout the structure and Q is the quality factor of the cavity with load from the beam [11]. The quality factor is a metric for how well the cavity retains its stored energy and can either be considered in isolation (unloaded) or with external loading from a circuit [12].

A fortunate property of the oscillating field is that the electron bunch will experience what is known as autophasing, meaning they will automatically adjust their phase to one suitable for the wave [3]. The principle itself can be explained as follows: suppose an ideal field strength exists such that particles gain just the right amount of energy to arrive at the same place in the next period. If the particles are not on this phase they will either gain more or less energy. Depending on the particle's phase relative to the wave, this will mean they either arrive earlier or later in the next period which will put them closer to or further from the ideal phase. Particles moving towards the ideal phase will thus oscillate around while those moving away will be lost. Figure 2.4 illustrates the concept over 2 sections where particles A and A' will experience a weaker field than the ideal over the first section, thereby arriving later in the second period. Meanwhile B and B' will experience the opposite. We note that only A' will be lost in this instance as it is moving away from the ideal phase. It is also worth mentioning that there exists two ideal phases however only one is stable.

2.1.4 Klystron and modulator

As previously mentioned the klystron is an RF-amplifier which serves to generate the power supplied to the accelerating structure [3]. It consists of a vacuum tube in which a small electron beam propagates, see Figure 2.5. RF-waves enter through the buncher-cavity, through which the electrons pass, causing energy modulation in the beam. This is due to the relative phase between electrons and RF-wave varying, meaning that different particles experience different field strengths such that they are either sped up or slowed down in the beam direction.

While in the drift space the continuous beam starts to bunch as faster electrons catch up with slower ones. The energy of the input field is thus stored within the potential of the beam and when passing the catcher-cavity, the now density modulated beam induces an amplified electromagnetic field [3, Ch. 4]. The amplified

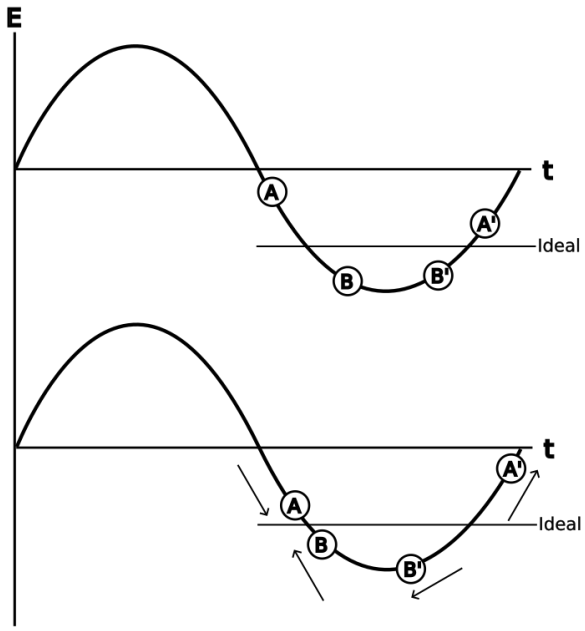

Figure 2.4: Example of autophasing [3]. Particles arriving close to the stable ideal phase will start oscillating around it while those arriving too late will be lost.

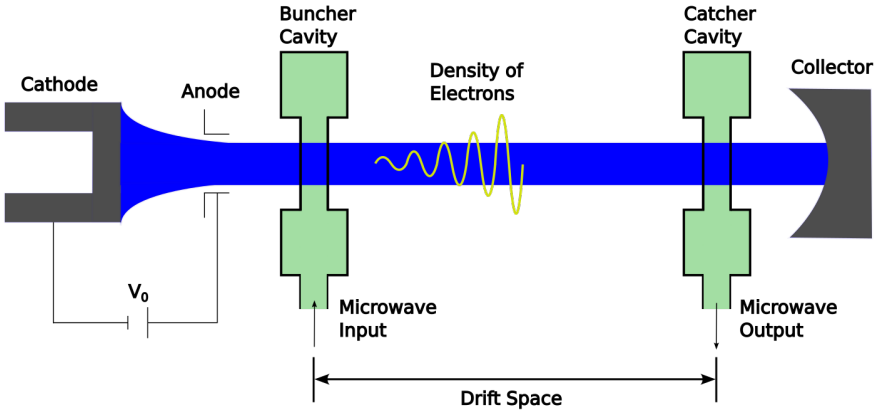

Figure 2.5: Layout of the klystron. The electron beam produced at the cathode will be density modulated by the RF inside the buncher cavity which will induce an amplified field in the catcher cavity.

signal can then be passed down the transfer line and into the SLED-cavity.

A limiting factor of the klystron output however is the non-linear behaviour it exhibits as the input power increases [13]. At a high enough power the electron beam modulation described above saturates, meaning the output power cannot be increased further by increasing the input.

In order to drive the high current electron beam within the klystron, a large voltage is needed which means the process would require enormous power if driven continuously [3, Ch. 7.6.5.]. Instead the amplification process is pulsed along with the RF-pulse using the aforementioned modulator as a power source, see Figure 2.6. The modulator uses a capacitor bank in order to build up a voltage over a longer period of time which can be emptied by triggering a switch, connecting the circuit and releasing a high voltage pulse. The 2.5 µs to 7.5 µs pulse passes through a transformer next, which further increases the voltage and allows it to power the klystron.

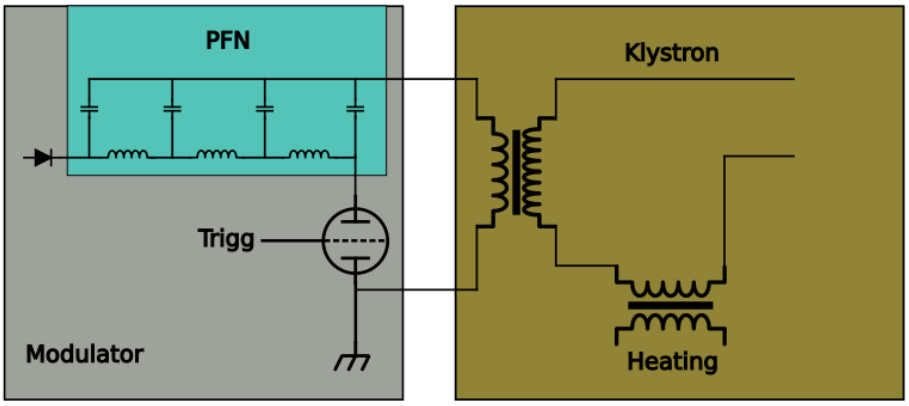

Figure 2.6: Circuit diagram of the modulator and klystron [3].

2.2 Pulse Compression

Before describing the SLED-cavity in full the principles of pulse compression will first be discussed in this section. Specifically how compression is applied in radar will be examined before connecting the ideas to the SLED.

2.2.1 Filters, Matched and SLED

In radar applications, pulse compression is used in order to decouple the undesired relationship between signal pulse width and range resolution [14, Ch. 20]. In such cases it is often the received signal that is compressed, usually through filtering. The filtered signal y can then be written as a convolution

$$y(t) = \int_{-\infty}^{\infty} h(t-\alpha)x(\alpha)\,d\alpha \tag{2.11}$$

between the received signal x and the linear filter h.

By choosing h in such a way as to maximize the signal-to-noise ratio (SNR) we get what is known as a matched filter. If the filter is chosen as the time-inversed complex conjugate of the output, $h(t) = ax^*(-t)$ for some arbitrary constant a, the convolution becomes

$$y(t) = \int_{-\infty}^{\infty} x^*(\alpha - t)x(\alpha)\, d\alpha \tag{2.12}$$

where we can also identify the filter as the autocorrelation of the received signal. As an example let us now examine a linear frequency modulated (LFM) signal

$$x(t) = \begin{cases} A\cos(\pi \frac{B}{\tau} t^2) & -\frac{\tau}{2} \leq t \leq \frac{\tau}{2} \\ 0 & \text{otherwise} \end{cases} \tag{2.13}$$

where A denotes the pulse amplitude, B the waveform bandwidth and τ the pulse length [14, Ch. 20]. A matched filter response will have an effective pulse width ($y(t) > -13.2\,\text{dB}$) of $\sim \frac{1}{B}$, yielding a compression ratio of τB. This can be seen as a fundamental limit on what can be achieved in terms of compression for a given bandwidth and initial pulse length. Note however that the filtered response pulse width assumes a large value for τB.

In the case of SLED the purpose of pulse compression is often not to maximize compression nor SNR. Rather, it is more desirable to dramatically increase the pulse amplitude over the last part of the pulse in order to fill the accelerating section. This is in order to increase the energy gained by the electrons and ensure consistent acceleration. As we see in Section 2.3 this is achieved over a pulsed step-response where the resonance of the cavities effectively act as a filter. While most literature does not directly address SLED as a filter, it is worth mentioning that it can be described as such. For an incident wave towards the SLED, the filter

$$h = \begin{cases} \alpha(\delta(t - t_0) + \frac{1}{T_c} e^{\frac{t_0 - t}{T_c}} - e^{\frac{t_0}{T_c}} \delta(t - t_0)) - \delta(t - t_0) & t_0 \leq t \\ 0 & t < t_0 \end{cases} \tag{2.14}$$

describes the output, not considering the travel-time for the wave within the structure. Here δ denotes the Dirac delta function, t_0 the starting time of the pulse and α and T_c are related to the SLED geometry discussed in Section 2.3.2.

Functionally, the SLED has an operating bandwidth of 1 MHz [4]. Comparing with the LFM this would translate to a maximum compression ratio $\tau B = 4$ for a 4 µs long pulse, which is close to what one usually aims for when using the phase-modulated RF wave.

2.3 The SLED-Cavity

In this section the SLED-cavity will be discussed in detail, including its structure and the mathematical theory behind it. This will prove vital in constructing a phase-modulation scheme and manipulating the outgoing wave to a desired form.

2.3.1 Structure

Initially developed at SLAC, Stanford, the SLED-cavity is a metal construction used for containing and compressing the incident electric field [2]. It consists of two cylindrical cavities attached to a waveguide system with a 3 dB coupler. A sketch of the SLED structure can be seen in Figure 2.7.

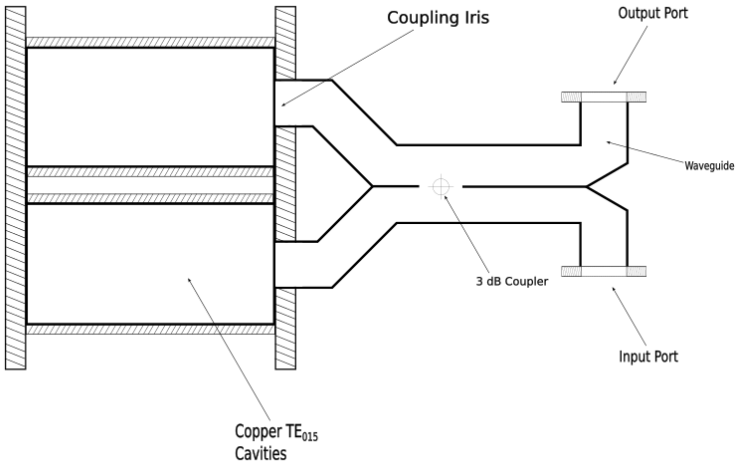

Figure 2.7: Layout of the SLED-cavity [2].

Let us begin with considering only one half of the structure, i.e. a waveguide connected to a resonant-cavity. The incident field from the klystron will enter through the input port and partially be reflected at the coupling iris at a 180° phase-shift [2]. The non-reflected field will enter into the cavity where it will be stored and the energy inside will grow over time.

By introducing the 3 dB coupler and a parallel waveguide the incident field will split at the coupler with a 90° phase-advance. When both fields get reflected at their respective iris, they return and pass through the 3 dB coupler, again with a 90° phase-advance. By summing the number of phase-advances we note that the 2 reflected waves cancel at the input port and add in the output port. This means we now have a structure which ensures the incident wave propagates forward, while also storing some of its energy inside the cavities.

Due to the open port at the entrance to the cavities, some of the stored field will start ”leaking” back out. This field will continue to grow as more energy is stored and have the same phase as the incident field, i.e. opposite the reflected wave, assuming the cavities are tuned to a resonance. By counting the number of phase-advances from the 3 dB coupler we see that these cavity fields also propagate into the forward port but add destructively to the reflected wave. Figure 2.8 shows how the envelope of the SLED-output evolves over time. Note how this is effectively the step response of the linear filter (2.14).

By now introducing a 180° phase-shift to the input, effectively inverting the

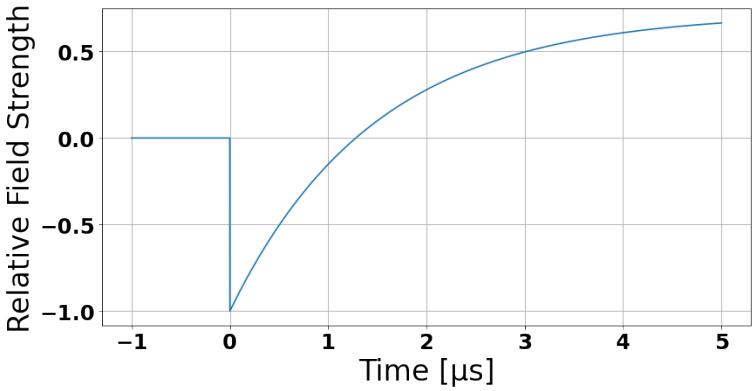

Figure 2.8: Field strength at the SLED-output for an incident RF-wave $E_i = 1$.

envelope, we are able to sharply increase the output as the rest of the system catches up. This is due to the difference in time it takes between the fields reflected at the iris and the cavities to transition phase. While the phase of the reflected wave will almost instantaneously shift along with the input, the wave inside the cavities will have a longer transition period. Because the new phase opposes the field stored inside the cavities, the energy within will start emptying out into the output port. During this transition period the 2 waves at the output will add constructively and the output amplitude will thus increase sharply before quickly decaying.

As the field within the cavities settles on the new phase, the cavities start storing up energy again and the output returns to destructive interference between the 2 waves. During normal operation the input is pulsed with the phase-shift happening towards the end, thereby effectively compressing the pulse. From the filter-perspective the process can be seen as 2 consecutive step-responses in opposite directions, see Figure 2.9.

2.3.2 Normal Operation

In order to establish a model for the sequence of events described above, let us again consider only a single cavity. Using the same notation as Farkas et. al. [2], we denote the emitted wave from the cavities by E_e, the incident wave as E_i, the reflected wave of the iris as E_K and the net reflected field E_L. For convenience we consider E_K as having the same magnitude as E_i but phase-reversed due to the reflection, and the net reflected field E_L as a superposition of E_e and E_K. We will only be accounting for the complex wave amplitude instead of the whole wave as the cavities are assumed to be resonant. It is now possible to set up the conservation of power

$$P_K = P_L + P_c + \frac{dW_c}{dt} \tag{2.15}$$

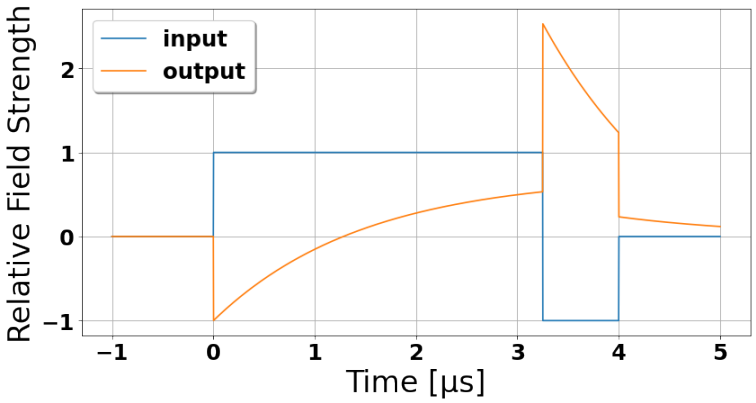

Figure 2.9: Input and output from the SLED filter. Here the input amplitude is set to $E_0 = 1$ and the behaviour of the output is described by (2.18).

for the cavities. Here P_K denotes the incident/reflected power, P_c the power lost due to dissipation inside the cavities and P_L, the net reflected power i.e. the power at the output port. W_c denotes the stored energy within the cavity. We now recall the relation between the stored energy and dissipated power for a resonator mentioned in Section 2.1.3, $P_c = \frac{\omega W_c}{Q_0}$. Note that ω refers to the angular frequency of the RF-power and Q_0 the unloaded quality factor. Let us introduce a coupling factor between cavity and iris β, such that the relation between dissipated power and emitted power from the cavities follows $P_e = \beta P_c$ [2]. Using the quadratic relation between field strength and power ($P \propto |E|^2$), we describe

$$|E_K|^2 = |E_e + E_K|^2 + \frac{|E_e|^2}{\beta} + \frac{2Q_0}{\omega\beta}\Re(E_e^* \frac{dE_e}{dt}) \tag{2.16}$$

and by expanding and rearranging terms, the result becomes a first order differential equation

$$T_c \frac{dE_e}{dt} + E_e = -\alpha E_K \tag{2.17}$$

Here the constants are bundled up into $T_c = \frac{2Q_0}{\omega(1+\beta)}$ and $\alpha = \frac{2\beta}{1+\beta}$. If the field strength E_K is kept constant, the differential equation has an exponential solution hence justifying naming T_c as the cavity filling time since the expression will have a term $\frac{t}{T_c}$.

Let us now consider the normal operation mode, where the input wave E_i is switched on at time t_0 and then phase-reversed by 180° at t_1 before being switched off at t_2. By only considering the wave-envelope we set $E_K = E_0 e^{i\phi(t)}$ where E_0 is the input field amplitude, $\phi = 180°\theta(t - t_1)$ and solve for E_e. The equations describing the total load field $E_L = E_e + E_K$ is then

$$E_L = \begin{cases} E_0 - \alpha E_0(1 - e^{-\frac{t-t_0}{T_c}}) & t_0 \leq t \leq t_1 \\ E_0(\alpha - 1) - \alpha E_0(2 - e^{-\frac{t_1-t_0}{T_c}})e^{-\frac{t-t_1}{T_c}} & t_1 \leq t \leq t_2 \\ \alpha E_0(1 - (2 - e^{-\frac{t_1-t_0}{T_c}})e^{-\frac{t_2-t_1}{T_c}})e^{-\frac{t-t_2}{T_c}} & t_2 \leq t \end{cases} \tag{2.18}$$

which separates the signal into three distinct parts like seen in Figure 2.9. In this example we set $E_0 = 1$, $t_0 = 0\,\mu s$, $t_1 = 3.25\,\mu s$ and $t_2 = 4\,\mu s$.

2.3.3 Alternative Operation Modes

Suppose now we switch the operating mode to that of a gradual phase-transition instead of the normal operation mode. In this mode we split the modulation into two parts: an initial phase-jump to ϕ_0 at $t = t_1$ similar to before, followed by a time-dependent phase-transition which gradually increases to 180° at t_{1b} [5]. The field is then cut off at t_2. An example of a linear modulation is given in Figure 2.10.

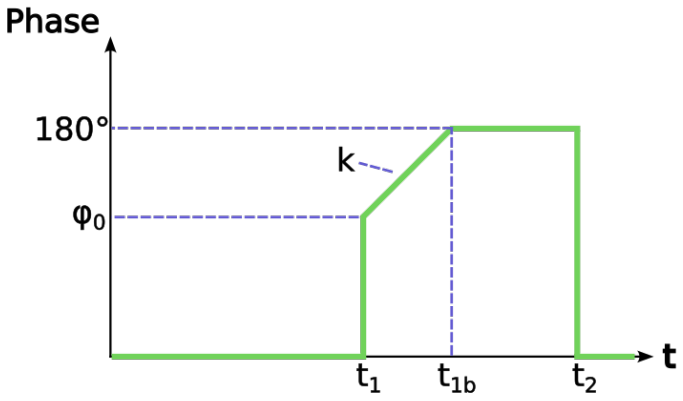

Figure 2.10: Example of a linear phase-modulation scheme [6]. An initial phase-shift takes place at time t_1 like in the normal operation mode, which linearly increases to 180° at t_{1b} where it remains constant.

We define the linear transition as $\phi(t) = \phi_0 + k(t - t_1)$ where $k = \frac{180° - \phi_0}{t_{1b} - t_1}$, and solve 2.17 to obtain the load field

$$E_L = \begin{cases} E_0 - \alpha E_0(1 - e^{-\frac{t-t_0}{T_c}}) & t_0 \leq t \leq t_1 \\ E_0 e^{i\phi(t)} + \alpha E_0[\frac{e^{\frac{t_1-t}{T_c}} e^{i\phi_0} - e^{i\phi(t)}}{1+jkT_c} + e^{\frac{t_1-t}{T_c}} + e^{-\frac{t}{T_c}}] & t_1 \leq t \leq t_{1b} \\ E_0 + \alpha E_0[\frac{e^{\frac{t_1-t_{1b}}{T_c}} e^{i\phi_0} + jkT_c}{1+jkT_c} e^{\frac{t_{1b}-t}{T_c}} - 1 + e^{\frac{t_1-t}{T_c}} - e^{-\frac{t}{T_c}}] & t_{1b} \leq t \leq t_2 \\ \alpha E_0 e^{\frac{t_2-t}{T_c}}[\frac{e^{\frac{t_1-t_{1b}}{T_c}} e^{i\phi_0} + jkT_c}{1+jkT_c} e^{\frac{t_{1b}-t_2}{T_c}} - 1 + e^{\frac{t_1-t_2}{T_c}} - e^{-\frac{t_2}{T_c}}] & t_2 \leq t \end{cases} \tag{2.19}$$

The result, as can be seen in Section 3.1, is a rounded off pulse with a reduced peak field. A disadvantage of this method however is that the phase throughout the SLED-pulse will vary along with the modulation meaning the electrons will exit the accelerating cavities with different phases. This is not much of a problem since the focus of the LINAC is to accelerate the particles, which will happen regardless due to the aforementioned auto-phasing phenomenon.

When considering the pulse-shaping made possible by dividing up the phase-modulation, one might consider if a flat-top on the outgoing pulse is achievable. This would allow for more consistent acceleration as the field strength would be the same regardless of the phase of the electrons. It has, in fact, been shown by several authors that this is possible but requires a non-linear phase-modulation [15, 16, 17]. We first expand the model to

$$T_c \frac{dE_e}{dt} + E_e(1 + iT_c\Delta\omega) = -\alpha E_K \tag{2.20}$$

in order to consider a small difference between the incoming RF frequency and the resonance frequency of the SLED-cavity $\Delta\omega$. This will add a term to the dissipation proportional to the frequency difference and allow for minimization of the phase-variation when reaching the flat-top[2].

By discretizing and rewriting $E_e = E_L - E_K$, we derive the update equation

$$E_{K_{n+1}} = E_{L_{n+1}} - E_{L_n}[1 - (1 + iT_c\Delta\omega)\frac{dt}{T_c}] + E_{K_n}[1 - (1 - \alpha + iT_c\Delta\omega)\frac{dt}{T_c}] \tag{2.21}$$

from which we then group the terms at time n into W_n such that $E_{K_{n+1}} = E_{L_{n+1}} - W_n$. We are then able to describe

$$|E_{L_{n+1}}|^2 = |E_{K_{n+1}}|^2 + |W_n|^2 + 2|E_{K_{n+1}}||W_n|\cos(\angle E_{K_{n+1}} - \angle W_n) \tag{2.22}$$

from which we note that W_n is equivalent to the cavity-field $E_{e_{n+1}}$.

Simply rearranging the terms now yields an update equation for the phase-modulation $\phi = \angle E_{K_{n+1}}$ which can be used in order to get the desired output $|E_{L_{n+1}}|$. Setting the load field constant between time t_1 and t_2 ($|E_{L_{n+1}}| = |E_{FLAT}|$) finally yields

$$\angle E_{K_{n+1}} = \arccos\left(\frac{|E_{FLAT}|^2 - |E_{K_{n+1}}|^2 - |W_n|^2}{2|E_{K_{n+1}}||W_n|}\right) + \angle W_n \tag{2.23}$$

which is the update equation needed in our case.

2.3.4 Energy Gain

In order to quantify how well adjusted a modulated travelling wave is to transferring energy to the electron bunch, we now derive the energy gain curve for a particle. The envelope of the wave will have a group-velocity separate from the speed of light as discussed in Section 2.1.3, which will decrease as it passes through

[2]While this method won't be utilized fully in this thesis, examples of such phase-minimization has been shown by Serpico et. al. [15].

the LINAC [18]. Since the MAX IV LINAC has a constant gradient throughout the accelerating structure, the group-velocity $v_g(z)$ will decrease linearly [4]. We can now define the travel time of the pulse, to any distance z along the accelerating structure

$$\Delta t(z) = -\frac{L}{g v_g(0)} ln\left(1 - g\frac{z}{L}\right) \tag{2.24}$$

starting from the input ($z = 0$). Note that $g = \frac{v_g(0) - v_g(L)}{v_g(0)}$ is the velocity gradient and L is the length of the accelerating section.

Defining $E_a(z,t)$ as the accelerating field along the structure, we note that the previous equation allows for the reduction $E_a(z,t) = E_a(0, t - \Delta t(z))$, assuming no interaction with the beam. It is clear that the structure has a filling time $T_a = \Delta t(L)$, and by now considering the SLED-pulse we set $E_a = E_L$. Assuming the electron traveling down the structure is relativistic (almost constant speed c), the energy gain when entering the structure at time t, $\Delta W(t)$, can be obtained by integrating over the whole structure

$$\Delta W(t) = q \cos\psi \int_0^L E_L(0, t - \Delta t(z) + \frac{z}{c})\, dz \tag{2.25}$$

Here q is the elementary charge, ψ the relative phase between particle and actual wave-top and the expression $\frac{z}{c}$ denotes the time it takes for a particle to travel the distance z at the speed of light c.

2.4 Phase-Modulation

This final section will present some basic forms of modulating a signal as well as describe how other accelerator facilities have implemented their phase-modulation solutions.

2.4.1 I/Q-Demodulation

While there are many ways of phase-modulating a signal electronically, a common method is so-called I/Q-demodulation. The abbreviation I/Q stands for "in-phase" and "quadrature", referring to how a wave can be described by an "in-phase" component and a 90° phase-shifted "quadrature". The idea of I/Q-demodulation is based on this principle and how the phase of an output-wave will depend on the I/Q components of the input. Suppose our input-wave is split (demodulated) into an I/Q-pair and amplified separately by a factor $I(t)$ for the "in-phase" and $Q(t)$ for the "quadrature". The equation

$$I(t)\cos\omega t + Q(t)\sin\omega t = \sqrt{I(t)^2 + Q(t)^2}\cos\left(\omega t + \arctan\left(\frac{Q(t)}{I(t)}\right)\right) \tag{2.26}$$

describes the output from recombining the signals (modulation). From this, it is clear that the amplifications I and Q will affect both the amplitude and phase of the output.

2.4.2 Hardware Implementations

As discussed in the introduction there have been several solutions made in order to modulate both the phase and amplitude of the incoming RF-waves for SLED operation. Modern solutions often employ a so-called digital low level RF (DLLRF) solution where the input is digitized and output is based on a control-loop along with an I/Q-modulator. This requires very fast ADCs and DACs along with very precise down-sampling in order to monitor the high-frequency RF.

An example of such an implementation is the LLRF system at the FERMI LINAC in Trieste which uses a linear phase-modulation scheme [19]. It employs a so-called field-programmable gate array (FPGA) as the main logic-unit, a semiconductor device with configurable logic blocks which allows the hardware itself to be reprogrammed [20]. An FPGA can thus be tailor-made to execute software efficiently and in parallel, making them significantly faster than a traditional CPU for specific tasks [21].

The unit handles both data processing from measurements along the transmission line as well as the pulse-to-pulse feed forward control algorithm. The whole system including the connected ADCs and DACs are synchronized on a single source, an over-controlled crystal oscillator (OCXO) which provides all the clock-frequencies to the system. It also provides a local oscillator (LO) at 2899 MHz for a mixer in order to down-convert the RF-frequency (2998 MHz) to a measurable signal with a specific sampling ratio.

This allows for precise knowledge of how the RF-signal is sampled meaning the behaviour of the sampling as well as the output can be characterized, eliminating the need for a very high sample-rate on the system. The output is in the form of an intermediate frequency (IF) generated by the DACs that together with the LO can be combined in another mixer to produce the final RF-frequency with the desired phase.

Another example can be found at the Diamond Light Source in Oxfordshire, UK where both amplitude and phase are modulated [8]. Similar to FERMI an FPGA is used to control and monitor the pulse travelling throughout the transmission line, however instead of the LLRF system producing the signal, it adjusts a vector modulator which controls phase and amplitude using I/Q-demodulation on the incoming signal. Software using PI-control determines appropriate I and Q outputs, and the result is a flat-top output similar to what was discussed in Section 2.3.3.

Chapter 3
Simulations and Construction

This chapter will detail the modelling and simulations made throughout the project and detail which model was chosen for implementation. Section 3.1 will examine some alternative operation modes and compare results followed by a deeper look into the linear operation. In Section 3.2, the electronic components chosen will be detailed along with necessary measurements made surrounding their properties. This will be followed by a description of the installation on one of the RF units for the LINAC along with the presentation of appropriate measurements.

3.1 Modelling

In order to determine an appropriate phase-modulation several models were created with adjusted parameters for the MAX IV RF-system, see Table 3.1. As pulse-length varies between the different RF-units it was decided that the model would be based on a 4 µs long RF-pulse based on previous work [4, 18]. Furthermore, all models were assumed to have a perfectly tuned SLED-cavity, i.e. $\Delta\omega = 0$ Hz.

Table 3.1: Relevant parameters for the MAX IV LINAC [4, 18].

Parameter	
RF Frequency	2.9985 GHz
Pulse Frequency	10 Hz
SLED Resonant Mode	TE_{015}
Unloaded Q_0	100000
Coupling Factor β	6.2
Cavity Filling Time T_c	1.47 µs
Accelerator Filling Time T_a	0.733 µs
Initial Group-Velocity $v_g(0)$	$0.037c$
Group-Velocity Gradient g	0.622
Length of S-band structure L	5.2 m

Equation (2.17) was solved for an input field of $E_K = e^{i\phi}$ and the load field E_L was computed for a step-wise, linear and a flat-top phase-modulation. The step-

wise modulation was based on the same scheme proposed by David Olsson et. al. [18] with time scheme $[t_0, t_1, ..., t_8] = [0\,\mu s, 3.25\,\mu s, 3.30\,\mu s, 3.35\,\mu s, 3.40\,\mu s, 3.45\,\mu s, 3.50\,\mu s, 3.55\,\mu s, 4\,\mu s]$ and phase-scheme $[\phi_0, \phi_1, ..., \phi_8] = [180°, 72°, 65°, 57°, 48°, 37°, 24°, 0°, 0°]$. For the linear modulation scheme, the times $[t_0, t_1, t_{1b}, t_2]$ were chosen as $[0\,\mu s, 3.25\,\mu s, 3.85\,\mu s, 4\,\mu s]$ and the initial phase-jump $\phi_0 = 110°$. Figure 3.1 shows the absolute value of the resulting load fields.

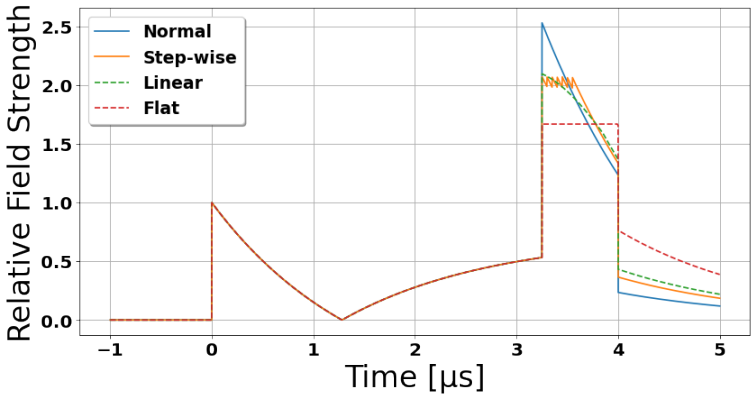

Figure 3.1: Comparison between load fields for normal, step-wise, linear and flat-top phase-modulation.

For the flat-top, a model of the load field was created and (2.23) was used to determine a suitable modulation scheme, see Figure 3.2. The maximum flat-top amplitude was determined empirically to be 1.67 times the input E_K as anything above would saturate the end-phase at 180° before the input-field is turned off. This in turn would cause the flat-top to decay, see Figure 3.3.

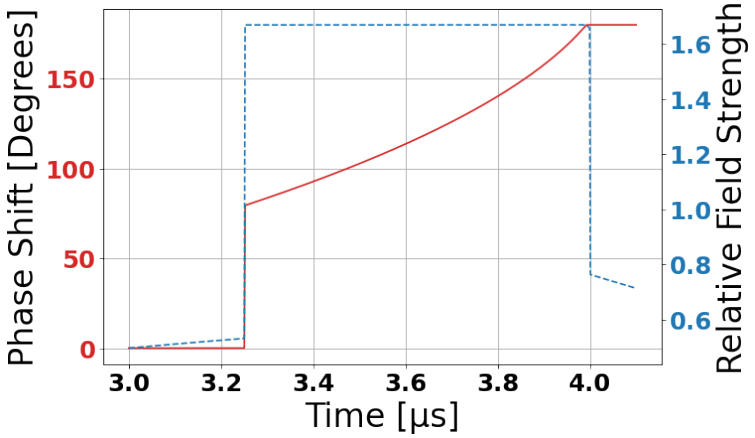

Figure 3.2: Phase-modulation (solid) and load field (dashed) for a flat-top.

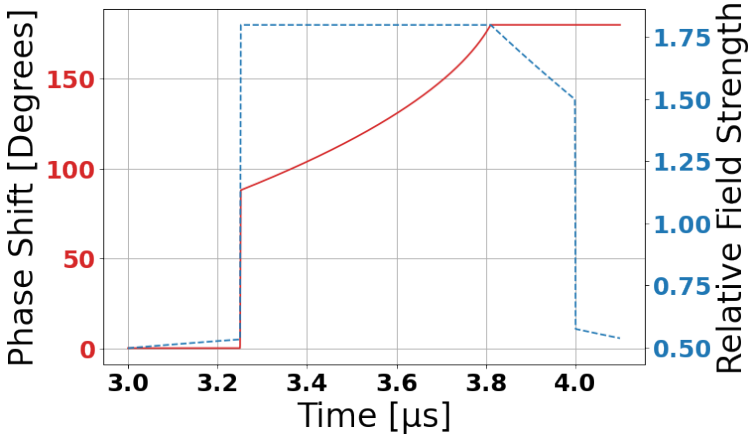

Figure 3.3: Phase-modulation (solid) and load field (dashed) with a decaying flat-top. A flat-top of 1.8 cannot be maintained for the whole duration.

Using (2.25), it was also possible to determine the energy gain for each case and calculate the maximum, see Figure 3.4. Note that the curves were normalized around the normal operation mode, eliminating the dependence on the electron-phase $\cos\psi$. The relative peak field reduction and peak energy gain were calculated

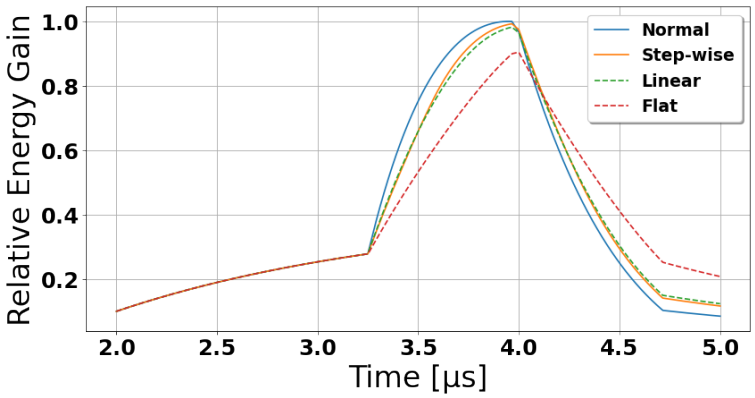

Figure 3.4: Comparison between energy gain curves for normal, step-wise, linear and flat-top phase-modulation.

and can be seen in Table 3.2.

After discussion with the RF-group at MAX IV as well as consultation with the RF-systems group at FERMI Elettra (Italy) it was eventually decided that a linear phase-modulation would be a realistic goal to implement. This decision was based on the availability of components in the lab as well as the precision-requirements being realistically achievable without an overly complex system. The

Table 3.2: Peak energy gain and peak field relative to the normal operation mode.

Operation Mode	Relative Energy Gain	Relative Peak Field
Normal	100%	100%
Step-wise	99.2%	81.8%
Linear	98.2%	82.8%
Flat-top	89.8%	65.5%

klystrons in the lab were also already operating in a saturated mode, meaning the significant loss in energy gain of the flat-top solution could not be compensated by increasing power.

Thus 2 factors needed to be determined, the initial phase-jump and the rise-time of the modulation. A comparison between simulations of different phase-jumps with a set 600 ns rise-time, as well as simulations of rise-times for a set phase-jump of 110°, can be found in Figures 3.5 and 3.6. Comparative energy gain curves can be seen in Figures 3.7 and 3.8, once again normalized around the normal operation mode.

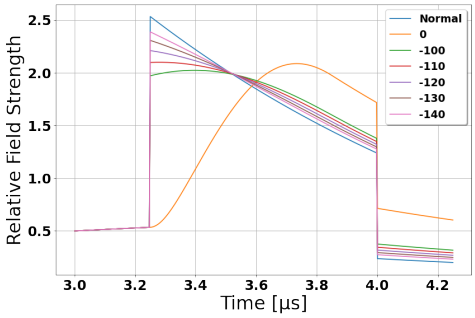

Figure 3.5: Comparison between load fields for different initial phase-jumps.

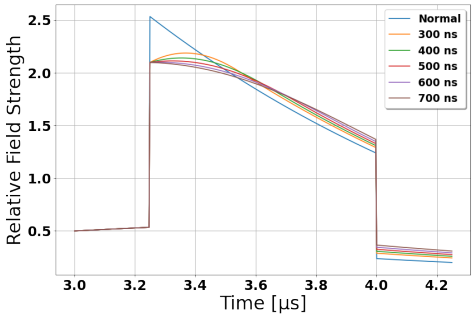

Figure 3.6: Comparison between load fields for different rise-times.

In consultation with the RF-group, a 110 degree phase-jump with a 600 ns rise-time was determined to be appropriate. This scheme would theoretically reduce peak fields by 18.2% and only yield a peak energy-loss of 1.8%.

3.2 Implementation

In order to implement the modeled phase-scheme it was decided that the current setup would be expanded instead of completely remodeled. The old discrete phase-shifter would be responsible for the initial phase-jump, while a newly added phase-shifter would cater to the ramping controlled by a micro-controller.

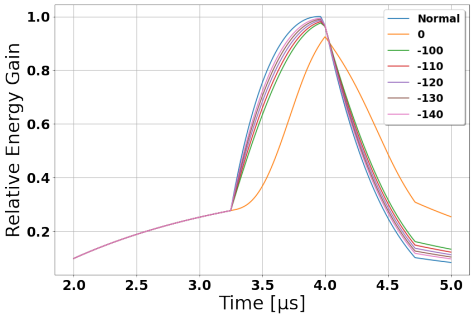

Figure 3.7: Comparison between energy gain curves for different initial phase-jumps.

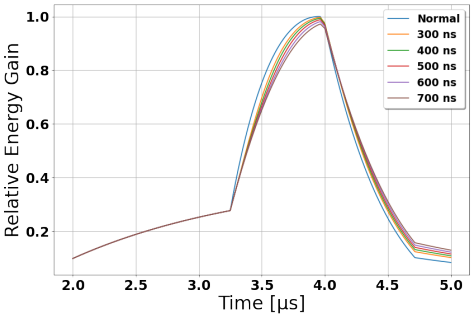

Figure 3.8: Comparison between energy gain curves for different rise-times.

3.2.1 The old setup

Every RF unit at MAX IV is already equipped with a fairly simple, analog phase-modulator setup. The components used are three splitters (two Mini-Circuits ZYSW-2-50DR and a ZAPDQ-4-s), one tuneable discrete phase-shifter (ARRA 9428B), one continuous phase-shifter (Clear Microwave PA2731) and a Traco Power voltage supply. The phase-shift by the ARRA 9428B is adjusted by a mechanical knob which changes the path-length of the transmission line, thereby altering the outgoing phase of the device [22]. Meanwhile, the Clear Microwave PA2731 is a varactor phase-shifter, meaning it uses a voltage-variable capacitor to adjust the circuit-impedance, affecting the phase of the outgoing wave. All circuitry is encased within a chassis with 4 inputs for RF, TTL and phase-adjustment along with one output for the shifted RF. Figure 3.9 displays the old setup.

RF is fed to the input marked RF IN and passes through the NO-line through to the output RF OUT where it proceeds to the klystron. When the trigger-signal is sent to produce the RF-pulse in the modulator, it is also fed to a digital delay generator (Stanford Research Systems DG645) which delays the signal to the desired time of phase-reversal t_1. A signal is then sent into the TTL2 channel which switches the line of the input RF to the NC-line at the second splitter. It thus bypasses the tuneable phase-shifter and exits through the same output, now shifted 180°. TTL1 is also governed by the delay generator and is capable of cutting off the pulse, ensuring the right pulse-length is passed through. The continuous phase-shifter acts as a corrector in order to match the whole signal to the general beam-phase.

3.2.2 The Phase-Shifters

The new phase-shifter solution was designed as follows: the old ARRA 9428B was re-tuned such that it would handle the initial phase-jump of 110°, while a newly added PA2731 would ramp the remaining 70° over 600 ns. This task-split was done to allow quick restoration of the original setup in case of failure, as well as to guarantee a stable initial phase-jump. The original PA2731 would still be

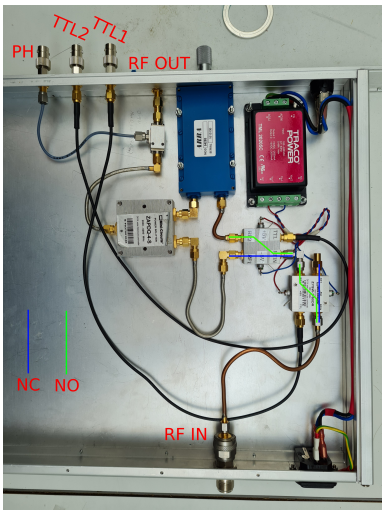

Figure 3.9: Current phase-modulator setup. The lines at the splitters marked NO/NC stand for normally opened/closed and are controlled by the TTL input. RF enters at the RF IN port and enters either the manual phase-shifter (NO) or bypasses it (NC) allowing for a phase-shift based on when a signal is sent to the TTL ports.

present, handling the phase-matching to the beam-phase. General parameters of the 2 models can be seen in Table 3.3.

Table 3.3: General parameters of the ARRA 9428B and the Clear Microwave PA2731 [23, 24, 25].

Parameter	ARRA 9428B	Clear Microwave PA2731
Frequency Range	DC - 18.0 GHz	2.7 - 3.1 GHz
Insertion Delay	0.68 - 0.78 ns	$\approx$ 100 ns
Insertion Loss	0.5 - 1 dB	3.6 - 3.8 dB
Phase-Range	180°	360°
Operating Voltage	-	0 - 9 V

In order to operate the PA2731, the phase-curve as a function of voltage had to be mapped out. This was done by connecting it to an RF signal generator and measuring the phase-difference over a period of time for different operating voltages on an oscilloscope. The applied voltage was also measured and adjusted between 0 V and 1 V in steps of 0.1 V with an additional measure at 0.05 V. Figure 3.10 shows the resulting curve from interpolating between the mean of 1000 measurements at each step with error bars depicting the phase-stability (standard deviation) of the phase-measurements.

The phase-stability average was 0.981°. A similar phase-measurement of the

setup without phase-shifter was also done to evaluate system-stability of the signal-generator. This yielded a standard deviation of 0.676°, which meant the true phase-stability of the PA2731 was 0.711°.

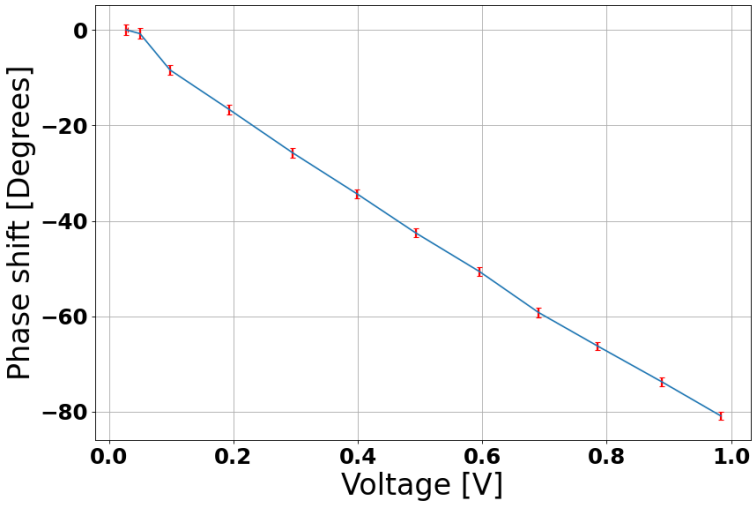

Figure 3.10: Phase-Voltage operating curve of the PA2731.

3.2.3 The Red Pitaya

The logic controller chosen to handle the linear phase-shift was a Red Pitaya STEMlab 125-14, a micro-computer with both a Dual-Core ARM Cortex-A9 MP-Core processor as well as a Xilinx Zynq 7010 FPGA [26]. It also came equipped with pre-installed SMA-contacts for RF-input/output at 14 bit, 125 MSa/s which could be used to output a pulsed ramping signal to the phase-shifter. The output was limited to 1 V, however as noted in the previous section the required voltage for the ramp was within this range.

The controller needed to handle a pulse-frequency of 10 Hz and respond to a trigger with very high consistency. This meant the controller needed a very fast response-time and could not require actions in-between pulses to take longer than 100 ms. By using FPGA-commands written by the manufacturer, the required logic was programmed directly onto the hardware, meaning the script only needed to be run once.

Commands to the FPGA were able to be sent either via running code directly on the board using the API or via the pre-installed SCPI-server. SCPI-commands allow for easy, remote control of a system using pre-defined commands sent via ASCII strings not too dissimilar from an API [27]. This method allowed for the control-logic to be written in Python and enabled easier access to the recorded data on the board.

Since the PA2731 exhibited linear behaviour within the working range, as seen in Figure 3.10, the output signal from the Red Pitaya was chosen so as to resemble Figure 2.10. The rise-time was set to 600 ns and the amplitude was empirically

tuned to 0.92 V by measuring the phase-shift on an oscilloscope. The pulse was set to trigger from the same delay generator that handled TTL1 and TTL2 and the delay was adjusted by hand in order to account for possible delays within the PA2731.

3.2.4 Installation

The new setup was installed and can be seen in Figure 3.11. Phase-stability was

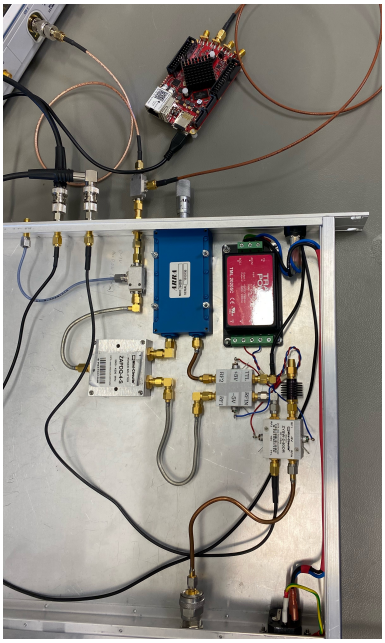

Figure 3.11: The new phase-modulator setup. The new PA2731 along with the logic controller can be seen at the end of the transmission (top side). Note that the trigger-input for the controller is missing in this image.

measured for both the old and new setup. This was done by connecting the old setup to a similar experimental station as before, with a signal generator and an oscilloscope measuring the phase between a reference wave and the output over 1000 measurements. Figure 3.12 shows the experimental setup for the new phase-modulator setup.

Stability before and after phase-shift were once again measured as the standard deviation of these measurement-series. The new system at full phase-shift was measured by applying a DC voltage at the planned amplitude of 0.92 V to the PA2731 while also switching on the TTL. The results can be seen in Table 3.4.

Finally the new phase-shifter system was installed on an RF-unit at the end of the LINAC and the output from the modulator, klystron, SLED and the reflected power towards the klystron were measured on an oscilloscope. Note that due to the high voltages the outputs were measured via rectifying diodes connected to

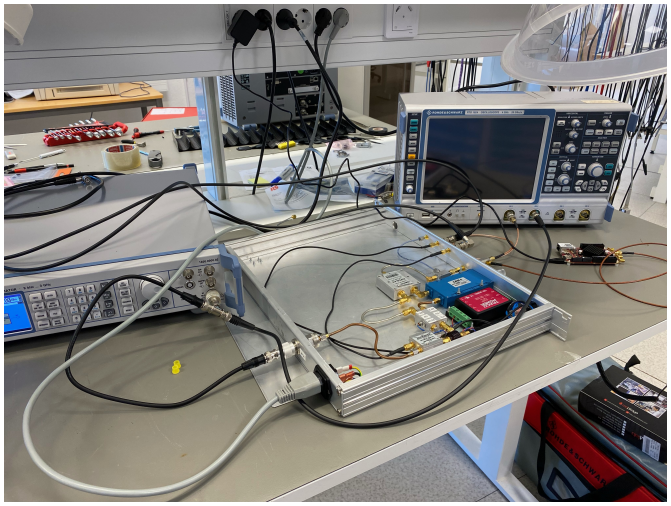

Figure 3.12: Experimental setup for measuring phase-stability. The signal generator (left) provides the RF to both the shifter and to the oscilloscope (right). The phase-difference can then be measured on the oscilloscope.

Table 3.4: Phase-stability Comparison.

Parameter	Standard Deviation σ
Old System 0°	1.688°
Old System 180°	1.660°
New System 0°	1.783°
New System 180°	1.749°

coaxial cables and damping components. As the damping-factors were unknown and differed between diodes, it was not possible to draw direct comparisons between the measured outputs of the klystron and SLED. The measurement-system did however allow for the signals to be measured simultaneously and in sync.

Figure 3.13 shows the output of the measured signals before changing phase-shifter system, Figure 3.14 the outputs given a phase-jump of 110° but no ramping and Figure 3.15 shows the new phase-shifter system. We observe that the modulator pulse (along the bottom) encapsulates the three other pulses, meaning the klystron is fully operational during the amplification process. We also note that a droop in the klystron output is present where we would expect a fairly rectangular pulse-shape. Along with this phenomenon, there also appears to be an increase in power reflected back towards the klystron. All cases feature the output of the SLED which exhibit behaviour similar to previous descriptions. For clarity Figure 3.16 shows the SLED-outputs for all three cases in one graph.

Unfortunately the RF-unit in question had just gotten its SLED-cavity installed, meaning the testing had to be done during conditioning of the vacuum at lower power and a shorter pulse length of 2 µs ($t_1 = 1.25\,\mu s$). Quick modelling of such a pulse showed the expected relative peak field to be 82.0%. It was also discovered that the cavities were no longer in tune meaning more power than expected was reflected back towards the klystron.

The peak field was measured for both the old and new phase-shifter systems and can be viewed in Table 3.5. It was not possible to measure the relative energy gain nor calculate it directly based on the pulse-shape since only the absolute value of the SLED-pulse was measured. By utilizing

$$\left| \int_0^L E_L(0, t - \Delta t(z) + \frac{z}{c})\, dz \right| \leq \int_0^L \left| E_L(0, t - \Delta t(z) + \frac{z}{c}) \right| dz \tag{3.1}$$

however, we can estimate an upper bound for the energy gain at the very least. The upper energy gain bound relative to normal operation was then determined, with E_L being the measured pulse-shapes (Old Setup, New Setup) in Figure 3.16.

Table 3.5: Upper energy gain bound and peak field relative to the normal operation mode for both modelled and measured outputs. Pulse length is 2 µs.

Operation Mode	Upper Energy Gain Bound	Relative Peak Field
Modelled Linear	100.6%	82.0%
Measured Linear	103.1%	79.4%

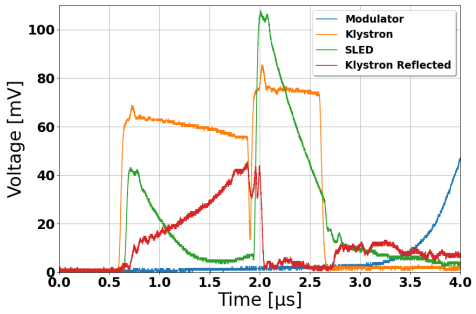

Figure 3.13: Measurements of the old phase-shifter system.

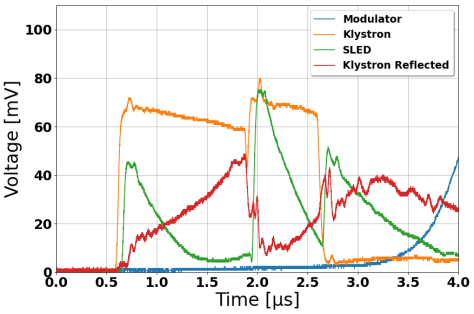

Figure 3.14: Measurements for only a $110°$ phase-jump.

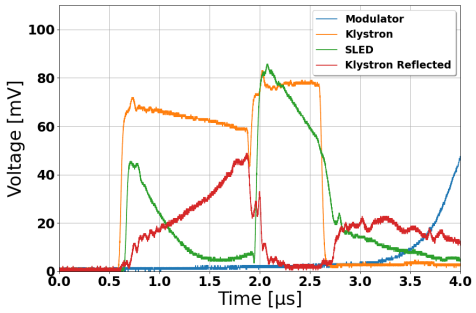

Figure 3.15: Measurements for the new phase-shifter system.

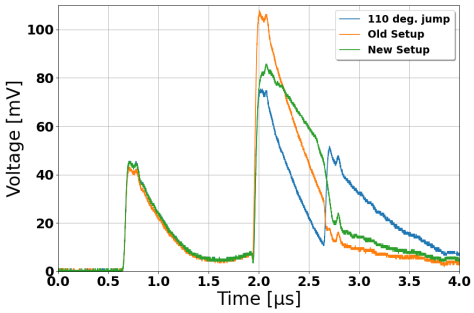

Figure 3.16: Direct comparison between SLED-outputs.

Chapter 4
Discussion

In this chapter the results from the implementation are discussed in regards to modelling, performance and stability.

4.1 Modelling

All modulation alternatives reduced the peak field compared to normal operation however the peak energy gain was also reduced. This is to be expected as anything below a 180° phase-shift for the incoming wave would mean the reflected wave and the wave from the cavities would still have some phase-mismatch at t_1. Both the step-wise and linear modulations managed to slow down the decay that follows from the cavities phase-transitioning. As the phase-shift reaches its maximum at t_{1b} however, they both decay in the same manner as in normal operation but with higher relative field strength.

Only the flat-top modulation remains unchanged between t_1 and t_2 as expected, however this comes at the cost of greatly reduced energy gain. From Figure 3.3 it is apparent that the phase-modulation is the limiting factor if one wants to increase the flat-top amplitude, since reaching 180° before the end of the pulse leads to decay. Increasing the phase-shift beyond 180° does not help either since we are limited by the phase of the wave inside the cavities.

The energy gain from each load field is also reflected in Figure 3.4 where both the step-wise and linear modulations share similar gain curves compared to normal operation. As the group-velocity decreases throughout the accelerating structure, a relativistic electron will "slip" forward relative to the pulse. Since the accelerator filling time T_a is close to the width of the compressed pulse, this means there should be a relatively well-defined maximum for the energy gain followed by a fast drop-off as the structure starts to empty. The peak in all cases is close to 3.9 µs which seems reasonable since most of the accelerating structure will then have been filled by the beginning of the compressed pulse ($t_1 + T_a \approx 3.98\,\mu s$). Due to the travel time of the electrons ($\frac{z}{c}$) the gain peak is shifted to slightly before the whole compressed pulse has entered the structure in all cases.

We also note that the flat-top modulation has an overall lower but symmetric gain peak that appears flat towards the end. This is indeed what we expected since the goal of a flat-top would be a pulse which is not as sensitive to the phase of the electrons. Unfortunately since the accelerator filling time is so long the

flat energy peak is very narrow which ultimately undermines the advantage of a flat-top modulation. This type of modulation would thus be more suited for an accelerating section with shorter filling time T_a which could be achieved by a higher group-velocity gradient or by shortening the section.

Table 3.2 shows the advantages and disadvantages of each operation mode. It is clear the linear modulation chosen for implementation performed worse than the step-wise modulation in both peak field reduction and energy gain retention but only by 1%. The linear modulation was deemed easier to implement since it would simplify the delay-timing to only 1 event (the ramping) when installed.

Having chosen a modulation scheme the next step was determining which parameters, rise-time and phase-jump, to choose. Looking at Figures 3.5 and 3.6 one clearly sees the influence the parameters have on the pulse-shape. A higher phase-jump would result in a stronger field strength at t_1 but a faster decay, while a shorter rise-time would similarly have a larger peak field in the first half of the pulse but also decay faster in the second half. As expected, having no phase-jump but instead ramping all 180° over 600 ns resulted in very low field strength at t_1 but instead a rounded top in the latter half of the pulse.

Figures 3.7 and 3.8 show that a larger phase-jump/shorter rise-time also yields higher peak energy gain. The standout case was once again the modulation with no phase-jump but a 180° ramp which had a noticeably worse energy gain curve than the rest. This highlights the need for an initial phase-jump since it allows the field strength to retain high values throughout the whole pulse.

A compromise had to then be made depending on how much energy gain could be lost and in the case of the MAX IV LINAC the klystron output was already in saturation. It was ultimately decided that the previously investigated linear modulation scheme would strike a good balance between these to factors.

4.2 Performance and Stability

As mentioned previously, the phase-stability was measured both before and after implementing the new system. The results showed that the new system performed somewhat worse in this regard and by using the values in Table 3.4 it can be estimated that the phase-shifter had a phase-stability of 0.563°. This was slightly smaller than expected given the measured phase-stability of the PA2731 being 0.711°. A possible explanation could be an insufficient measurement setup, where the remaining components within the setup such as the splitters were the cause of most of the phase-instability. Regardless it seems reasonable to conclude that the phase-stability has worsened somewhat however this does not appear to have hindered performance.

When applied to the real transmission line the phase-shifter system performed close to expectations despite the conditions of the testing not being ideal. It was expected that some power would be reflected back towards the klystron since the cavities in the SLED cannot be tuned perfectly. Looking at Figures 3.13 through 3.15 however, it seems enough power was reflected to interfere with the outgoing klystron pulse, reducing the amplitude mid-pulse. As mentioned previously no direct comparisons should be made between the amplitudes in these figures but

it is clear that the ”droop” in the klystron pulse corresponds to the rise in reflected power. There were attempts at correcting the resonance by re-adjusting the water-cooling system attached to the cavities but it soon became evident that mechanical re-tuning would be necessary. For lack of time it was therefore decided that measurements would be carried out before re-tuning.

In Figure 3.16 it is evident that the modulation of the phase has a large impact on the shape of the outgoing SLED-pulse. By only shifting 110° the cavities do not empty completely, instead releasing the remaining energy once the klystron pulse is cut off. This is visible past the klystron pulse cut-off ($t > 2.5\,\mu s$) as an increase in both the SLED-output and the reflected klystron power. Ramping the remaining 70° did indeed yield a higher peak field which was still reduced compared to normal operation and we achieved behaviour in accordance with theory. In the end, the peak field was reduced to 79.4% which is slightly below the expected value of 82.0%.

A possible source of error would of course be insufficient modelling of the cavities due to the assumption of tuned cavities no longer holding true. It was also discovered that the signal-strength to the oscilloscope was very sensitive to movement of the attached damping-devices. While caution was taken not to alter the measurement setup, human errors could have occurred during adjustments of the new phase-shifter system which would have affected the signal strength. This may also explain why there are some small differences in the klystron output pulse between Figures 3.13 through 3.15.

Another surprising result was that the upper energy gain bound was higher in both the modelled and measured cases for the linear modulation. As mentioned in Section 2.3.3 the phase of the wave will vary along with the modulation. By only considering the absolute value of the pulse this information is lost, meaning only the area covered by each pulse matters. This unfortunately means that it is difficult determine anything concrete regarding the relative loss in energy gain. It stands to reason however that losses should be close to theory, similar to the peak field, as the pulse envelope appears fairly similar to what was conceived during modelling.

Chapter 5
Conclusion

The MAX IV LINAC has been in need of an improved RF-system to reduce the peak fields throughout the transmission line. This has been achieved by introducing a linear phase-modulation to the RF-signal entering the SLED-cavity, based on a similar solution at FERMI Elettra, Trieste Italy. Simulations for the desired model yielded a peak field reduction to around 82.8% of the normal operation mode while only loosing 1.8% of the energy gain.

In reality the peak field was reduced by 79.4% but this was in part due to the divergence from the theoretical parameters used during modelling. Measurements seemed to indicate that the overall phase-stability had worsened somewhat however this does not appear to have had any major effects on the performance of the new phase-shifter system. The overall pulse shape from the new phase-shifting system appears to overlap well with theory and the system appears stable. Further testing is needed once the cavities are re-tuned and the conditioning of the vacuum is finished.

Chapter 6
Future Work

Regarding further development there are many ways of expanding and improving the system. Suggestions are as follows:

- Try swapping the phase-shifter to an I/Q-modulator and demodulator in order to more precisely control the amplitude of the RF, as well as allow for more arbitrary phase-modulation schemes by adjusting the I/Q-ratio. This would require some rewriting of the logic for the controller but should be realistically achievable with the Red Pitaya.
- Implement a pulse-to-pulse feedforward system by sampling the RF signal before and after phase-shift. A possible way to do this would be to follow the example at FERMI where a mixer is used to lower the frequency in order to avoid aliasing. Unfortunately the RF-system at MAX IV does not currently have access to an alternative RF-signal so another option would be to mix the input signal with the output after the phase-shifter. This should result in a voltage corresponding to a certain shift and the behaviour could be mapped through experiments.
- Re-purpose the current RF-generator into an LO with an up-scaling mixer, such that the RF fed into the klystron could be generated directly from the control-unit. This would allow direct manipulation of the signal generation from the controller, which could improve stability and allow for the possibility of an arbitrary phase-modulation. Realistically speaking however this is not feasible at the moment, as it would require reworking large parts of the RF-system.

Bibliography

[1] J.V. Lebacqz. "High power klystrons". In: *IEEE Transactions on Nuclear Science* 12.3 (1965), pp. 86–95.

[2] Z.D. Farkas et al. "SLED: A method of doubling SLAC's energy". In: *Proc. Of 9th Int. Conf. On High Energy Accelerators, SLAC*. 1974, p. 576.

[3] S. Werin. *Accelerator Technique 2.5th Edition*. MAX-lab, 2006.

[4] MAX-Lab. *MAX IV Detailed Design Report*. Lund University, Sweden. 2010. URL: https://www.maxiv.lu.se/beamlines-accelerators/accelerators/accelerator-documentation-2/.

[5] D. Wang et al. "Phase Modulation SLED Mode on BTW Sections at Elettra". In: *Proceedings of PAC*. 2009.

[6] C. Serpico et al. "Phase Modulation SLED Operation Mode at Elettra". In: *Proceedings of IPAC* (2011), p. 83.

[7] G. Shu et al. "RF modulation studies on an S band pulse compressor". In: *Chinese Physics C* 40.3 (2016), p. 037002.

[8] C. Christou, P. Gu, A. Tropp, et al. "Programmable SLED System for Single Bunch and Multibunch Linac Operation". In: *JACoW* LINAC2022 (2022), MOPOJO19. DOI: 10.18429/JACoW-LINAC2022-MOPOJO19.

[9] D.J. Griffiths. *Introduction to electrodynamics*. Cambridge University Press, 2018. ISBN: 9781108420419.

[10] A. Karlsson and G. Kristensson. *Microwave theory*. English. Lund University, Lund, 2015.

[11] M. Weiss. *Introduction to RF linear accelerators*. CERN, 1994.

[12] T.H. Lee. *The design of CMOS radio-frequency integrated circuits*. Cambridge University Press, 2004. ISBN: 9780521835398.

[13] R. Yogi and C. Martins. "Energy Efficient Klystron Operation at Saturation: Possibility due to Novel Modulator". In: *2019 International Vacuum Electronics Conference (IVEC)*. 2019, pp. 1–3. DOI: 10.1109/IVEC.2019.8745026.

[14] M.A. Richards, J. Scheer, and W.A. Holm. *Principles of modern radar*. Radar, Sonar, Navigation and Avionics. SciTech Pub., 2010. ISBN: 9781891121524.

[15] C. Serpico, M. Dal Forno, A. Fabris, et al. "Optimization of the SLED phase modulation parameters of the FERMI linac". In: *Proceedings of the North American Particle Accelerator Conference (Pasadena, USA, 2013)*. 2013, pp. 981–983.

[16] S.H. Shaker et al. "Phase modulator programming to get flat pulses with desired length and power from the CTF3 pulse compressors". In: *IPAC* 10 (2010), pp. 1425–1427.

[17] A. Fiebig and Ch. Schieblich. *A SLED type pulse compressor with rectangular pulse shape*. Tech. rep. CERN, 1990.

[18] D. Olsson, P. Lilja, and L. Malmgren. "Increasing the Photon Energy for Photonuclear Experiments in MAX-lab by Phase Modulating the SLED Pulse". In: *Technical Report LUTEDX/(TEAT-7242)/1-11/(2016)* 7242 (2016).

[19] A. Fabris et al. "The LLRF system for the S-band RF plants of the FERMI Linac". In: *IEEE Transactions on Nuclear Science* 63.2 (2016), pp. 861–868.

[20] AMD Xilinx. *What is an FPGA?* URL: https://www.xilinx.com/products/silicon-devices/fpga/what-is-an-fpga.html (visited on 03/23/2023).

[21] *FPGA explained in simple words*. URL: https://hardwarebee.com/fpga-explained-in-simple-words/ (visited on 03/23/2023).

[22] *Phase Shifters*. URL: https://www.microwaves101.com/encyclopedias/phase-shifters (visited on 04/18/2023).

[23] *Mail correspondence with Clear Microwave Support*.

[24] *PA2731 Data Sheet*. URL: http://www.clearmicrowave.com/phase_shifters.htm (visited on 04/18/2023).

[25] *ARRA 9428B General Specifications*. URL: http://www.arra.com/coaxial-components/phase-shifters/motorized-phase-shifter/motorized-phase-shifters-dc-18-ghz.html (visited on 04/18/2023).

[26] *STEMlab 125-14 Technical Specifications*. URL: https://redpitaya.com/stemlab-125-14/ (visited on 04/18/2023).

[27] *Introducing SCPI Commands*. URL: https://www.rohde-schwarz.com/us/driver-pages/remote-control/remote-programming-environments_231250.html (visited on 04/18/2023).

Printed by Tryckeriet i E-huset, Lund 2023

LUND
UNIVERSITY

Series of Master´s theses
Department of Electrical and Information Technology
LU/LTH-EIT 2023-921
http://www.eit.lth.se